

Finite element analysis of nonreciprocal phase shift for TE-modes in magneto-optic rib-waveguides with a compensation wall

N. Bahlmann, M. Lohmeyer, H. Dötsch and P. Hertel
University of Osnabrück, 49069 Osnabrück, Germany

July 21, 1998

Abstract

The nonreciprocal phase shift for TE-modes in magneto-optic rib-waveguides supporting a domain lattice was recently predicted. Using a single magnetic compensation wall in the symmetry-axis of the waveguides, the nonreciprocal phase shift can be enhanced by a factor up to 1.8. The nonreciprocal phase shift is calculated by perturbation theory. The electromagnetic fields are determined by a semi-vectorial finite element method, which properly handles the required field discontinuities.

1 Introduction

For the development of polarization independent magneto-optic devices it is desired to have nonreciprocal waveguides for TM as well as for TE-modes. The nonreciprocal phase shift of TM-modes was predicted by Yamamoto et al. [1] several years ago. Different waveguides showing a nonreciprocal phase shift for TM-modes were studied experimentally [2, 3]. Recently, Popkov et al. [4] predicted the nonreciprocal phase shift for TE-modes in gyrotropic rib waveguides with a normally magnetized domain lattice.

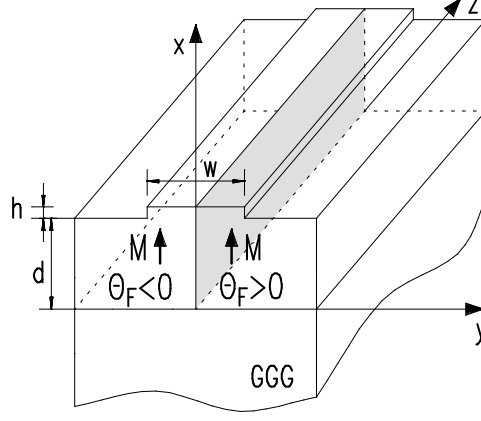
In this paper we report on nonreciprocal waveguides using a magnetic compensation wall [5] at the center of the rib waveguides. The magnetization is adjusted in the entire waveguide parallel to the film normal. Only the Faraday rotation changes the sign at the compensation wall so that an asymmetry, which is essential for nonreciprocity, is induced.

To calculate the unperturbed TE-mode fields we employ a new semi-vectorial finite element method, which properly takes care of the field discontinuity at the waveguide boundaries. The nonreciprocal phase shift is derived in perturbation theory. It is shown that the maximum nonreciprocal phase shift can be enhanced by a factor 1.3 to 1.8 as compared with waveguides supporting a domain lattice.

2 Nonreciprocal Rib Waveguides

The following analysis is performed for the basic rib geometry sketched in Fig. 1. Mode propagation is assumed along the z axis and the entire waveguide is magnetized parallel

Figure 1: Basic geometry of the rib waveguides with a compensation wall.



to the film normal. A compensation wall divides the rib waveguide into two equal halves with opposite sign of the Faraday rotation, which is the basis of the nonreciprocal effect. The piecewise constant dielectric tensor can be written as a sum of the dielectric and the small magneto-optic part

$$\hat{\epsilon} = \hat{\epsilon}_0 + \Delta\hat{\epsilon} = \begin{pmatrix} \epsilon & 0 & 0 \\ 0 & \epsilon & 0 \\ 0 & 0 & \epsilon \end{pmatrix} + \begin{pmatrix} 0 & 0 & 0 \\ 0 & 0 & i\xi \\ 0 & -i\xi & 0 \end{pmatrix}. \quad (2.1)$$

The gyrotropy is represented by ξ , being related to the Faraday rotation Θ_F by

$$\xi \approx 2n\Theta_F/k_0, \quad (2.2)$$

where n is the refractive index and k_0 is the vacuum wave number.

The mode propagation in the waveguides is described by Maxwell's equations. As the magneto-optic effect is small, the nonreciprocal phase shift $\Delta\beta = \beta_{\text{fw}} - \beta_{\text{bw}}$, which is the difference between the forward and backward propagation constants β_{fw} and β_{bw} of the TE-mode, can be derived with perturbation theory [1, 4]. Assuming the semi-vectorial approximation ($E_x = 0$) [6], perturbation theory yields

$$\Delta\beta = 2\omega\epsilon_0 \frac{\iint \vec{E}^* \Delta\hat{\epsilon} \vec{E} dx dy}{\iint \{\vec{E} \times \vec{H}^* + \vec{E}^* \times \vec{H}\}_z dx dy} = \frac{k_0^2 \iint \xi E_y (\partial_y E_y) dx dy}{\beta^2 \iint \{E_y^2 - \frac{1}{\beta^2} E_y (\partial_y^2 E_y)\} dx dy}. \quad (2.3)$$

Since ξ is a piecewise constant function and E_y is piecewise defined, the integration in y -direction can be performed analytically, giving the squared modulus of E_y times the jump of ξ at the vertical interfaces. Then the numerator of equ. 2.3 is written as follows

$$\frac{1}{2} \int_0^{d+h} \Delta\xi_{y=0} E_y^2(x, 0) dx - \frac{1}{2} \int_d^{d+h} [\Delta\xi_{y=-w/2} E_y^2(x, -w/2) - \Delta\xi_{y=w/2} E_y^2(x, w/2)] dx \quad (2.4)$$

where $\Delta\xi_{y=i} = \xi_{y<i} - \xi_{y>i}$ denotes the jump of ξ at the vertical boundary at $y = i$. As the field E_y is discontinuous at the rib flanks the second term in eq. 2.4 must be evaluated with fields inside the ribs.

To determine the unperturbed modal field distribution $E_y(x, y)$ of the TE modes in the semi-vectorial approximation we have to solve the mode equation

$$(-\partial_x^2 - \partial_y^2 - \epsilon k_0^2 + \beta^2) E_y = 0 \quad (2.5)$$

for E_y in the computational window Ω . Furthermore we have to regard the boundary conditions for E_y at horizontal (Γ_{hor}) and vertical boundaries (Γ_{ver}), resp. and on the

boundary of the computational window (Γ). On the horizontal boundaries the field E_y and the derivative $\partial_x E_y$ must be continuous. For vertical boundaries we enforce the continuity of ϵE_y and $\partial_y E_y$ [6]. We get

$$\begin{aligned}
E_y &= 0 && \text{on } \Gamma, \\
\left. \begin{aligned} E_{y,t} - \phi_{\text{hor}} &= 0 \text{ and } E_{y,b} - \phi_{\text{hor}} = 0 \\ (\partial_x E_y)_t - q_{\text{hor}} &= 0 \text{ and } (\partial_x E_y)_b - q_{\text{hor}} = 0 \end{aligned} \right\} && \text{on } \Gamma_{\text{hor}} \text{ and} \\
\left. \begin{aligned} \epsilon_l E_{y,l} - \phi_{\text{ver}} &= 0 \text{ and } \epsilon_r E_{y,r} - \phi_{\text{ver}} = 0 \\ (\partial_y E_y)_l - q_{\text{ver}} &= 0 \text{ and } (\partial_y E_y)_r - q_{\text{ver}} = 0 \end{aligned} \right\} && \text{on } \Gamma_{\text{ver}}.
\end{aligned} \tag{2.6}$$

The indices t, b, l and r indicate the top, bottom, left and right side of the respective boundary (see Fig. 2). ϕ and q describe the corresponding boundary conditions. With this notation the weak form of the differential equation can be written as follows [7]:

$$\begin{aligned}
& \int_{\Omega} v(-\partial_x^2 - \partial_y^2 - \epsilon k_0^2 + \beta^2) E_y d\Omega + \int_{\Gamma} \bar{v} E_y d\Gamma \\
& + \int_{\Gamma_{\text{hor}}} \bar{v}_t [(\partial_x E_y)_t - q_{\text{hor}}] - \bar{v}_b [(\partial_x E_y)_b - q_{\text{hor}}] + \bar{v}_t (E_{y,t} - \phi_{\text{hor}}) - \bar{v}_b (E_{y,b} - \phi_{\text{hor}}) d\Gamma \\
& + \int_{\Gamma_{\text{ver}}} \bar{v}_l [(\partial_y E_y)_l - q_{\text{ver}}] - \bar{v}_r [(\partial_y E_y)_r - q_{\text{ver}}] + \bar{v}_l (\epsilon_l E_{y,l} - \phi_{\text{ver}}) - \bar{v}_r (\epsilon_r E_{y,r} - \phi_{\text{ver}}) d\Gamma = 0.
\end{aligned} \tag{2.7}$$

If this equation holds for every testfunction v and \bar{v} , E_y is a solution of the differential equation respecting all continuity requirements. Partial integration of the first term yields

$$\begin{aligned}
\int_{\Omega} v(-\partial_x^2 - \partial_y^2 - \epsilon k_0^2 + \beta^2) E_y d\Omega &= \int_{\Omega} (\partial_x v \partial_x E_y + \partial_y v \partial_y E_y - \epsilon k_0^2 v E_y + \beta^2 v E_y) d\Omega \\
- \int_{\Gamma} v \vec{n} \nabla E_y d\Gamma &- \int_{\Gamma_{\text{hor}}} (v_t (\partial_x E_y)_t - v_b (\partial_x E_y)_b) d\Gamma - \int_{\Gamma_{\text{ver}}} (v_l (\partial_y E_y)_l - v_r (\partial_y E_y)_r) d\Gamma,
\end{aligned} \tag{2.8}$$

where \vec{n} is the normal vector on the boundary. Inserting this into equation 2.7 and choosing

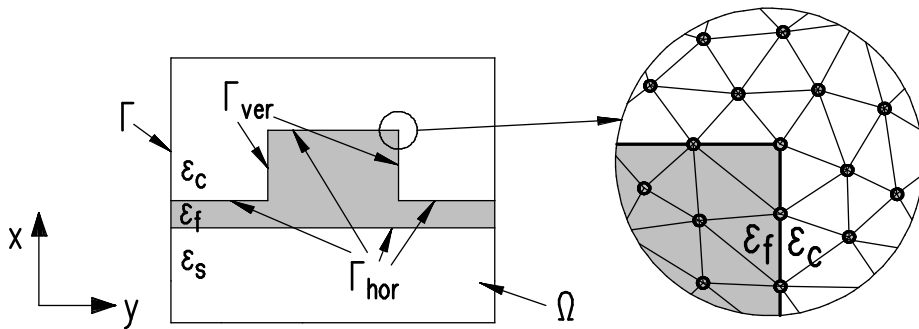


Figure 2: Illustration of the different boundaries for the FEM calculations.

$v = \bar{v}$, which can be done without loss of generality, we arrive at the simple form

$$\begin{aligned} & \int_{\Omega} (\partial_x v \partial_x E_y + \partial_y v \partial_y E_y - \epsilon k_0^2 v E_y + \beta^2 v E_y) d\Omega + \int_{\Gamma} (v E_y - v \vec{n} \nabla E_y) d\Gamma \\ & + \int_{\Gamma_{\text{hor}}} [-(v_t - v_b) q_{\text{hor}} - (v_t - v_b) \phi_{\text{hor}} + (v_t E_{y,t} - v_b E_{y,b})] d\Gamma \\ & + \int_{\Gamma_{\text{ver}}} [-(v_l - v_r) q_{\text{ver}} - (v_l - v_r) \phi_{\text{ver}} + (v_l \epsilon_l E_{y,l} - v_r \epsilon_r E_{y,r})] d\Gamma = 0 \quad \forall v. \end{aligned} \quad (2.9)$$

For the finite element solution of this problem, we expand E_y in a set of expansion functions N on first order triangular elements, $E_y = \sum a_i N_i$ (see Fig. 2). The coefficients a_i represent the field value at the node i . With special restrictions to the function space the above integral form can be further simplified. The integral over the boundary of the computational window Γ vanishes if the v_i and N_i are set to zero on Γ . On the horizontal boundaries Γ_{hor} we choose the test and expansion functions to coincide, $v_i \equiv N_i$. They are continuous at the boundary, so that the respective integral is zero, too, because of $v_t = v_b$ and $E_{y,t} = E_{y,b}$. In contrast to this situation and the most common finite element algorithms, we use different functions v_i and N_i at the vertical boundaries Γ_{ver} . The N_i must be discontinuous ($N_{i,l} = \epsilon_r / \epsilon_l N_{i,r}$) in order to provide the correct jump for E_y at this boundary [8]. On the other hand, the v_i must be continuous, so that the derivative of E_y becomes continuous. Then the relevant integral in equation 2.9 over Γ_{ver} vanishes.

Now we can write equation 2.9 as an eigenvalue equation

$$\hat{K} \vec{a} = -\beta^2 \hat{M} \vec{a} \quad (2.10)$$

where the matrix elements of \hat{K} and \hat{M} correspond to the respective parts of the first integral in eq. 2.9 and the elements of \vec{a} describe the value of E_y on the nodal points. This eigenvalue equation has been solved with commercial software [9].

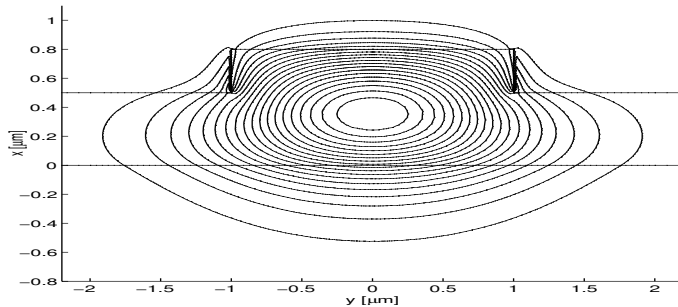
3 Results

Using this formalism we compute the nonreciprocal phase shift for different geometries of the waveguides in order to optimize the absolute value of $\Delta\beta$. The material parameters, $n_{\text{substrate}} = 1.9$, $n_{\text{film}} = 2.2$, $n_{\text{cover}} = 1.0$ and $\Theta_{\text{F}} = 3000^\circ/\text{cm} \Rightarrow \xi = 0.005$, are identical with those used by Popkov et al. [4]. They are typical for epitaxially grown bismuth substituted iron garnet films. The wavelength is $1.3 \mu\text{m}$.

Figure 3 shows the calculated mode field of the fundamental TE-mode. Note the typical discontinuities of E_y at the rib flanks. The computational window ($12 \mu\text{m} \times 6 \mu\text{m}$) is divided into 21798 triangles. The mesh is chosen denser in the region where the field strength is large. This region can be estimated by simple effective index calculations so that we get a quasi adaptive mesh.

The nonreciprocal phase shift of the fundamental TE-mode for waveguides with a compensation wall as well as for waveguides supporting a domain lattice is plotted in fig. 4 for a constant film thickness $d = 0.3 \mu\text{m}$. The thick lines indicate that only the fundamental TE-mode is guided. In the other region the mode solver finds at least two guided TE-modes. The nonreciprocal phase shift increases understandably with the rib height since the numerator of equ. 2.3 grows with better localization of the mode. For waveguides with a compensation wall the nonreciprocal phase shift is always larger than for waveguides

Figure 3: Contour plot of the field component $|E_y|$ of the fundamental TE-mode. The contour levels are spaced by 5% of the maximum field amplitude. The geometry is equal to that in [4] ($d = 0.5 \mu\text{m}$, $h = 0.3 \mu\text{m}$, $w = 2.0 \mu\text{m}$).



with a magnetic domain lattice. Besides, the maximum for waveguides with a compensation wall is in all cases in the single mode regime. This is important for future isolator applications.

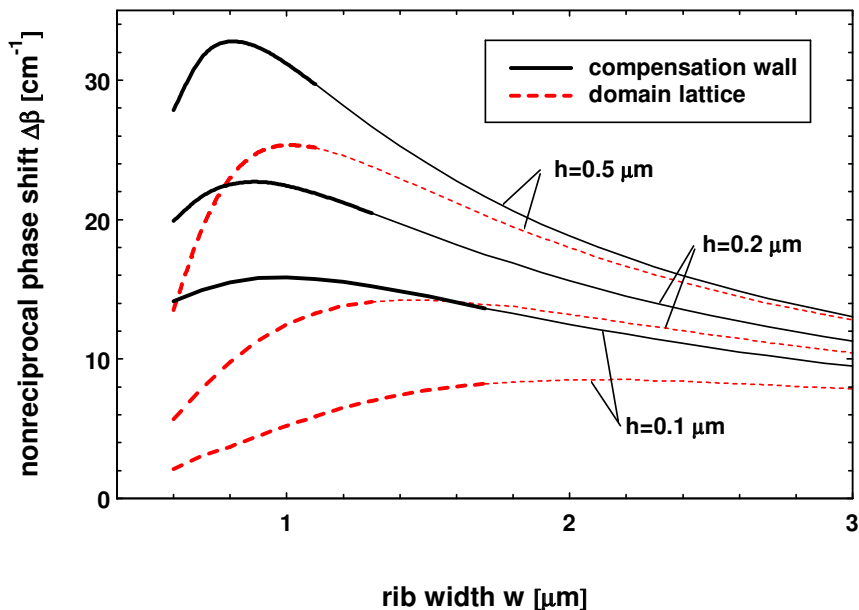


Figure 4: The nonreciprocal phase shift of the fundamental TE-mode in waveguides with a compensation wall or a domain lattice for different rib heights h versus the rib width w . The film thickness is $d = 0.3 \mu\text{m}$. Thick lines indicate that only the fundamental mode is guided. Thin lines represent solutions where at least one more guided TE-mode is found.

In order to estimate the accuracy of the semi-vectorial finite element calculation we computed the same waveguides additionally with a simple scalar finite element [10] and another semi-vectorial method, the so called wave matching method [11]. The results for the nonreciprocal phase shift and the propagation constants of the zero order TE-mode are shown in fig. 5 and fig. 6. Obviously the results of both semi-vectorial computations agree both closely, while the scalar approximation deviates considerably. Only for weakly etched ($h = 0.1 \mu\text{m}$) and narrow ($w < 0.9 \mu\text{m}$) ribs differences between semi-vectorial results occur. This discrepancy results from a different lateral size of the calculated mode distributions. Although the computational window for the FEM is chosen to be large that it has no influence on the mode fields, the computed modes extend not as far as those calculated by the WMM-method. The reason for this is not yet known and has no influence on the determined propagation constants β of the modes as shown in fig.6. Figs. 5 and 6 indicate that different mode solvers should be compared not only with respect to the effective mode indices, but also with respect to expressions like (2.3, 2.4) that rely on

precisely calculated mode fields.

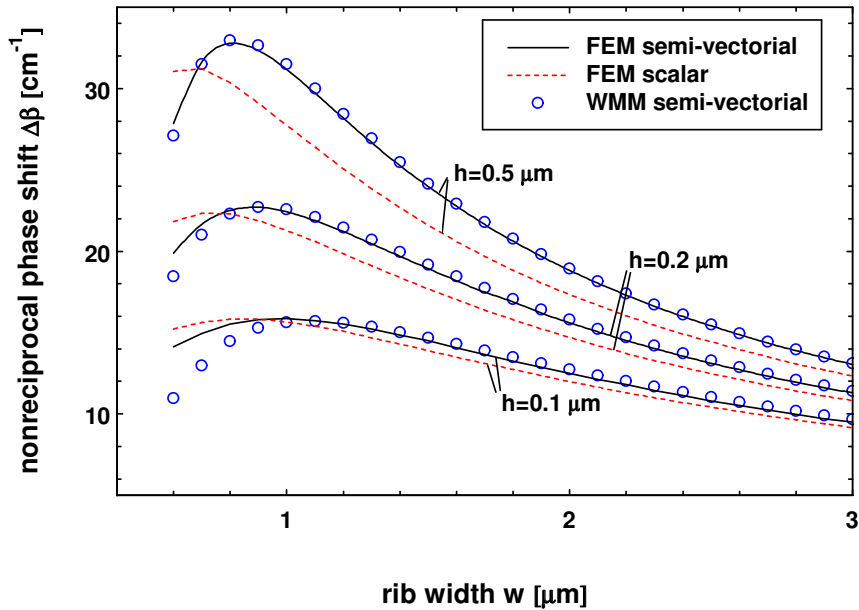


Figure 5: Nonreciprocal phase shift of the fundamental TE-mode in waveguides with a compensation wall computed with three different mode solvers. The film thickness is $d = 0.3 \mu\text{m}$.

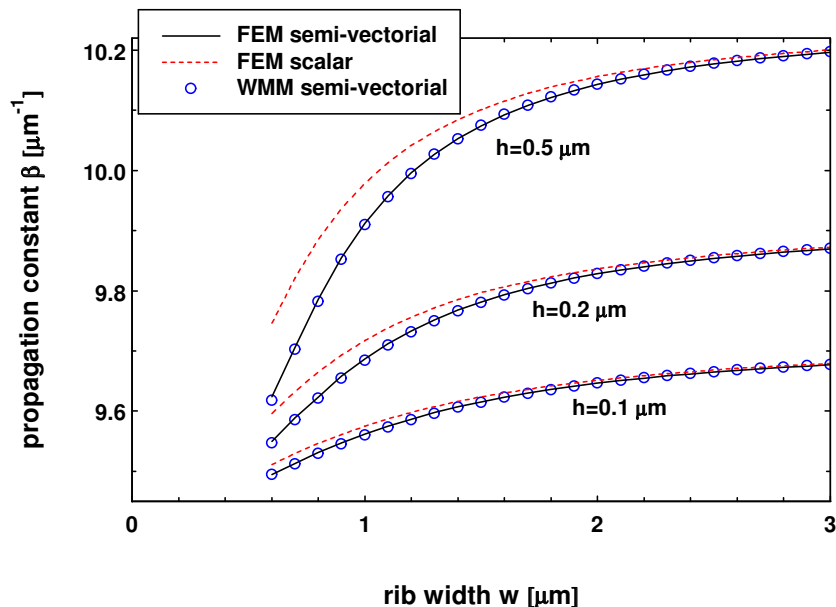


Figure 6: Propagation constant β_{TE} for a film thickness of $d = 0.3 \mu\text{m}$. Results from a scalar FEM, the semi-vectorial WMM and our new approach are shown.

4 Summary

In this paper we have proposed a new semi-vectorial finite element method to calculate the TE-mode fields in rectangular rib waveguides which properly handles all continuity requirements of Maxwell's equations. Using these mode distributions, the nonreciprocal phase shift of TE-modes in waveguides with a compensation wall can be computed

by means of perturbation theory. Such waveguides are required for polarization independent or TE-mode integrated optical isolators. The results show that the maximum nonreciprocal phase shift can be enhanced by a factor 1.3 up to 1.8 as compared with waveguides with a magnetic domain lattice. Comparing with results obtained by another semi-vectorial mode solver shows an excellent agreement.

Acknowledgements

We gratefully acknowledge financial support by Deutsche Forschungsgemeinschaft, Sonderforschungsbereich 225.

References

- [1] S. Yamamoto and T. Makimoto, "Circuit theory for a class of anisotropic and gyrotropic thin-film optical waveguides and design of nonreciprocal devices for integrated optics," *Journal of Applied Optics*, vol. 45, no. 2, pp. 882–888, 1974.
- [2] T. Shintaku, T. Uno, and M. Kobayashi, "Magneto-optic channel waveguides in Ce-substituted yttrium iron garnet," *Journal of Applied Physics*, vol. 74, no. 8, pp. 4877–4881, 1993.
- [3] N. Bahlmann, V. Chandrasekhara, A. Erdmann, R. Gerhardt, P. Hertel, R. Lehmann, D. Salz, F. Schröteler, M. Wallenhorst, and H. Dötsch, "Improved design of magneto-optic rib waveguides for optical isolators," *Journal of Lightwave Technology*, vol. 16, no. 5, pp. 818–823, 1998.
- [4] A. F. Popkov, M. Fehndrich, M. Lohmeyer, and H. Dötsch, "Nonreciprocal TE-mode phase shift by domain walls in magneto-optic rib waveguides," *Applied Physics Letters*, vol. 72, no. 20, pp. 2508–2510, 1998.
- [5] J.-P. Krumme and P. Hansen, "New magneto-optic memory concept based on compensation wall domains," *Applied Physics Letters*, vol. 23, no. 10, pp. 576–578, 1973.
- [6] M. S. Stern, "Semivectorial polarised finite difference method for optical waveguides with arbitrary index profiles," *IEE Proceedings*, vol. 135, Pt. J, no. 1, pp. 56–63, 1988.
- [7] Olgierd C. Zienkiewicz, *The Finite Element Method*, McGraw-Hill Book Company (UK) Limited, Maidenhead Berkshire, England, third edition, 1977.
- [8] M. Koshiba, K. Hayata, and M. Suzuki, "Finite-Element Formulation in Terms of the Electric-Field Vector for Electromagnetic Waveguide Problems," *IEEE Transactions on Microwave Theory and Techniques*, vol. 33, no. 10, pp. 900–905, 1985.
- [9] The MathWorks Team, *Partial Differential Equation Toolbox For Use with MATLAB*, The MathWorks Inc., Natick, Mass., 1995.
- [10] N. Mabaya, P.E. Lagasse, and P. Vandenbulcke, "Finite Element Analysis of Optical Waveguides," *IEEE Transactions on Microwave Theory and Techniques*, vol. MTT-29, no. 6, pp. 600–605, 1981.

- [11] M. Lohmeyer, “Wave-matching method for mode analysis of dielectric waveguides,” *Optical and Quantum Electronics*, vol. 29, pp. 907–922, 1997.